Nano Research
2019, 12(4): 863–868

ISSN 1998-0124 CN 11-5974/O4
https://doi.org/10.1007/s12274-019-2313-z

Research Article

Bioengineered magnetoferritin nanozymes for pathological identification of high-risk and ruptured atherosclerotic plaques in humans

Tao Wang[1,§], Jiuyang He[2,3,§], Demin Duan[3], Bing Jiang[3], Peixia Wang[3], Kelong Fan[3], Minmin Liang[3] (✉), and Xiyun Yan[3] (✉)

[1] *Department of Neurosurgery, Peking University Third Hospital, Beijing 100191, China*
[2] *Savaid Medical School, University of Chinese Academy of Sciences, Beijing 100049, China*
[3] *Key Laboratory of Protein and Peptide Pharmaceutical, Institute of Biophysics, Chinese Academy of Sciences, Beijing 100101, China*
[§] *Tao Wang and Jiuyang He contributed equally to this work.*

Received: 7 December 2018 / **Revised:** 23 January 2019 / **Accepted:** 29 January 2019

ABSTRACT

Atherosclerotic plaque rupture results in thrombus formation and vessel occlusion, and is the leading cause of death worldwide. There is a pressing need to identify plaque vulnerability for the treatment of carotid and coronary artery diseases. Nanomaterials with enzyme-like properties have attracted significant interest by providing biological, diagnostic and prognostic information about the diseases. Here we showed that bioengineered magnetoferritin nanoparticles (M-HFn NPs) functionally mimic peroxidase enzyme and can intrinsically recognize plaque-infiltrated active macrophages, which drive atherosclerotic plaque progression and rupture and are significantly associated with the plaque vulnerability. The M-HFn nanozymes catalyze the oxidation of colorimetric substrates to give a color reaction that visualizes the recognized active macrophages for one-step pathological identification of plaque vulnerability. We examined 50 carotid endarterectomy specimens from patients with symptomatic carotid disease and demonstrated that the M-HFn nanozymes could distinguish active macrophage infiltration in ruptured and high-risk plaque tissues, and M-HFn staining displayed a significant correlation with plaque vulnerability (r = 0.89, P < 0.0001).

KEYWORDS

atherosclerosis, high-risk plaques, ruptured plaques, magnetoferritin nanoparticles, nanozymes, pathological diagnosis

1 Introduction

Atherosclerosis is a disease of the arterial wall, where endothelial cell damage results in the accumulation of lipids and inflammatory cells within discrete areas of the intima, eventually forming atherosclerotic plaques within the vessel lumen [1–5]. Macrophage-rich inflammation is an obligatory component of active plaques that contributes to lesion ruptures and triggers acute myocardial infarction and stroke [6–8]. Visualization of vascular inflammation and identification of ruptured and high-risk plaques thus represent a major clinical advance for prevention and treatment of coronary and carotid artery diseases [9–12].

Nanomaterials have emerged as a favorite approach to characterize plaque-infiltrated macrophages given their natural specificity for macrophages and unique physicochemical properties [13–15]. Meanwhile, nanomaterials with intrinsic enzyme-like characteristics has attracted significant interest by providing biological [16–19], diagnostic [20–22] and prognostic information [23] about the diseases. We first reported the intrinsic enzyme-like activity of Fe_3O_4 nanoparticles (NPs) in 2007 [24] and subsequently developed a number of nanozyme-based approaches for biological detection [25, 26], disease diagnosis [27, 28], and medicine development [29, 30]. In this study, we demonstrated that the bioengineered magnetoferritin nanoparticles (M-HFn NPs) exhibit remarkable peroxidase-like activity that can simultaneously recognize and visualize macrophages within plaque specimens from patients with symptomatic carotid disease for pathological identification of ruptured and high-risk plaques.

2 Results

2.1 Preparation and enzyme-like activity characterization

We expressed recombinant human HFn nanocages from *E. coli*, as described previously [31]. M-HFn NPs were prepared by loading Fe^{2+} into the cavities of HFn nanocages through the iron ion channel on the surface of HFn nanocage, followed by the formation of an iron oxide nanocore within HFn nanocage by oxidation in the presence of H_2O_2 (Fig. 1(a)). After purification, the bioengineered M-HFn NPs were thoroughly characterized by various methods. Cryo-electron microscopy (cryo-EM) images showed the formation of the uniformly spherical and monodispersed nanocores with an average diameter of ~ 4.3 nm that are clearly encapsulated within the HFn nanocages (Fig. 1(b)). Dynamic light scattering (DLS) characterization further confirmed the prepared M-HFn NPs are monodispersed with identical diameters before and after forming iron oxide nanocore within HFn nanocage (Fig. 1(c)). X-ray diffraction pattern (JCPDS No. 85-1436) further confirmed the formation of Fe_3O_4 nanocores within the HFn nanocages (Fig. 1(d)). The CD spectra of M-HFn NPs were almost identical to that of HFn protein nanocages (Fig. 1(e)), indicating that iron loading did not significantly perturb the structural conformation of HFn nanocages, implying that HFn refolds into their native state upon the loading process.

M-HFn NPs catalyzed the oxidation of commonly used peroxidase colorimetric substrates TMB, DAB or OPD in the presence of H_2O_2 to give an intense color reaction (Fig. 2(a)), showing the remarkable

Address correspondence to Minmin Liang, mmliang@ibp.ac.cn; Xiyun Yan, yanxy@ibp.ac.cn

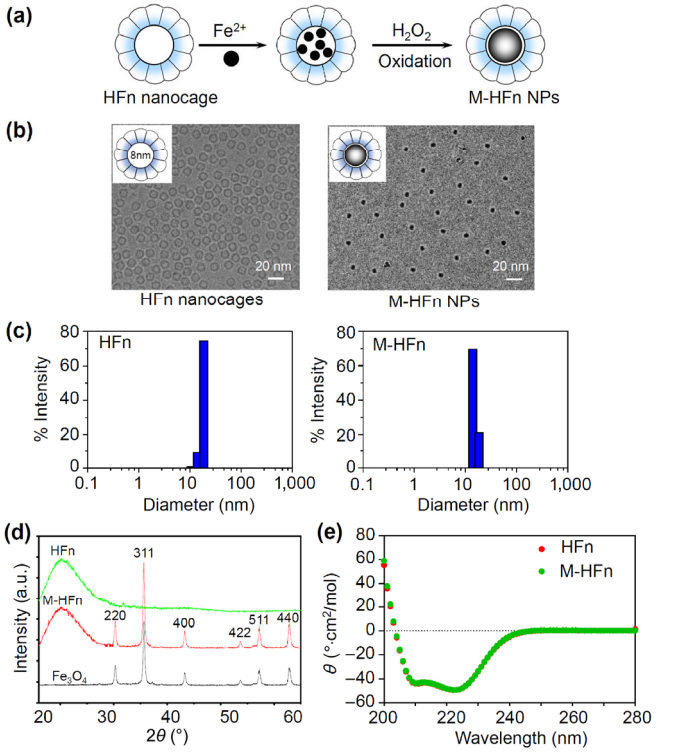

Figure 1 Preparation and characterization of M-HFn NPs. (a) Schematic diagram depicting the preparation of M-HFn NPs and their structure. (b) Cryo-EM image of HFn nanocages (left) and M-HFn NPs (right). (c) DLS characterization of HFn nanocages (left) and M-HFn NPs (right). (d) XRD pattern of M-HFn NPs. (e) CD spectra of HFn nanocages and M-HFn NPs showing no secondary structure change to the HFn protein nanocage after iron loading.

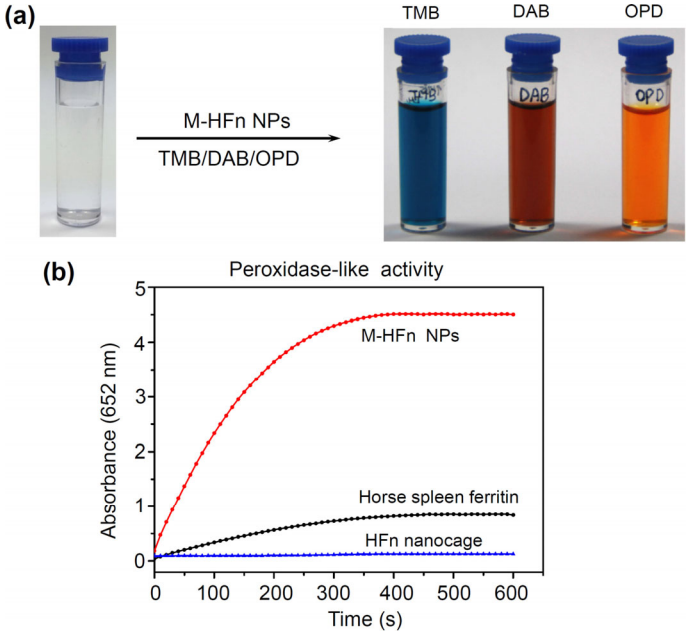

Figure 2 Peroxidase-like catalytic activity of M-HFn NPs. (a) M-HFn NPs show peroxidase-like activity by catalyzing the oxidation of peroxidase substrates (TMB, DAB and OPD) to produce colorimetric reactions. (b) Reaction-time curves of the TMB colorimetric reaction catalyzed by M-HFn NPs, horse spleen ferritin with ferrihydrite ($5Fe_2O_3·9H_2O$) nanocores, and HFn nanocage without iron oxide core, respectively.

peroxidase-like catalytic activity of M-HFn nanozymes. Figure 2(b) further demonstrated the typical reaction-time curves of TMB colorimetric reaction catalyzed by M-HFn nanozymes. The results indicate that the mineral phase composition of the iron core determines the peroxidase-like activity of M-HFn nanozymes. M-HFn with mineral cores consisting of magnetite (Fe_3O_4) exhibited a much higher peroxidase activity while compared with natural ferritin with encapsulated ferrihydrite ($5Fe_2O_3·9H_2O$) core. HFn nanocages, without mineral core, exhibited no peroxidase activity.

2.2 M-HFn nanozymes specifically stain unstable and ruptured plaques in humans

Patients were predominantly old-aged men with multiple cerebrovascular risk factors. Carotid atherosclerotic plaques were resected from all patients by carotid endarterectomy operation. To demonstrate that M-HFn nanozymes can specifically stain high-risk and ruptured atherosclerotic plaques, we pathologically examined paraffin-embedded carotid sections using M-HFn staining. As shown in Fig. 3, we compared 20 stable and 30 unstable/ruptured carotid artery atherosclerotic plaques. We employed hematoxylin-eosin staining for morphologic characterization and Masson staining for collagen distribution identification. In the unstable ruptured plaques, M-HFn staining was extensive and occurred mostly near the thin ruptured fibrous cap (Fig. 3(a)). In contrast, little staining was observed in the stable plaques (Fig. 3(b)). The quantitative analysis of M-HFn nanozyme-positive staining areas in stable and unstable ruptured plaques revealed significantly higher area density (positively stained proportion of evaluated area) in unstable ruptured plaques than in stable plaques (Fig. 4(a)), and M-HFn staining displayed a significant correlation with plaque vulnerability ($r = 0.89$, $P < 0.0001$) (Fig. 4(b)). The results show that M-HFn staining can be used as a clinical index for pathological identification of human plaque vulnerability.

2.3 Binding specificity of human HFn to plaque macrophages

Macrophage-rich inflammation is an obligatory component of active atherosclerotic plaques and is particularly intense in high-risk unstable plaques [5, 32]. Plaque-infiltrated macrophages have been established as an indicator for identifying plaque vulnerability [33, 34]. Herein, we demonstrated that M-HFn nanozyme selectively stains unstable and ruptured plaques via specific binding to plaque-infiltrated macrophages. Since iron loading into the cavity of HFn nanocages

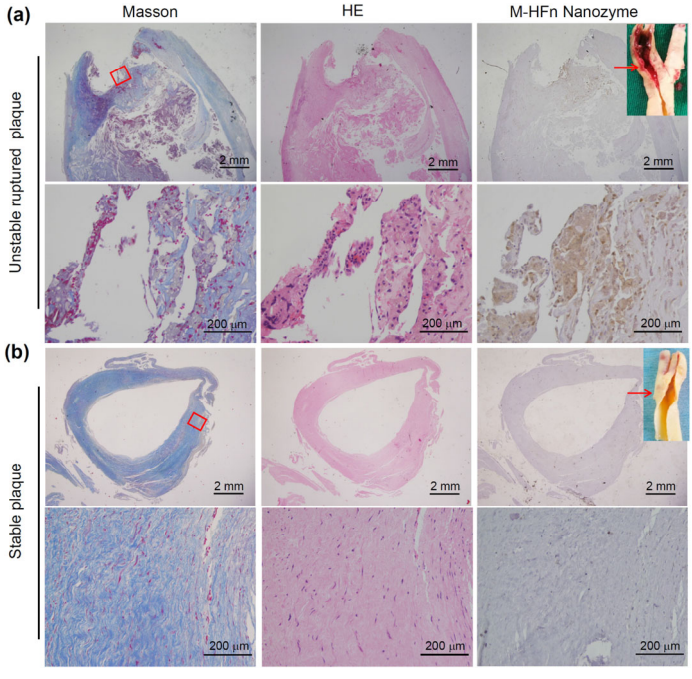

Figure 3 M-HFn nanozymes specifically stain the unstable and ruptured plaques. Paraffin-embedded carotid sections were stained by HE, Masson, or M-HFn nanozymes. Unstable and ruptured plaque tissues showed extensive positive staining for M-HFn nanozymes (a), whereas the stable plaques were negative for M-HFn staining (b). Arrows indicate the histological section position.

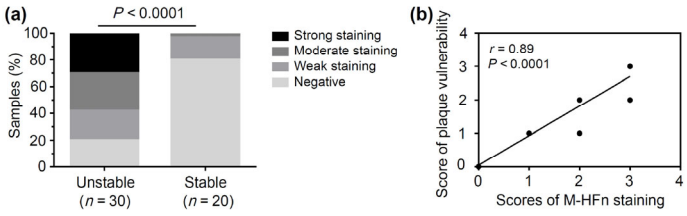

Figure 4 M-HFn staining can be used as a clinical index for human unstable and ruptured plaque identification. (a) M-HFn staining of plaque tissues. The staining was scored as negative (0; < 10% staining), weak (1; 10%–25% staining), moderate (2; 25%–50% staining) and strong (3; > 50% staining). (b) Quantitative analysis of the stained sections showed that M-HFn staining was significantly correlated with plaque vulnerability (*** $P < 0.0001$, $r = 0.89$; Pearson's correlation). Two trained observers scored the plaque vulnerability on an ordinal scale (0–3) based on the presence of two key components of vulnerable plaques, intraplaque hemorrhage and inflammation (CD 68 staining). A score of 0 represented no hemosiderin or inflammation, 1 was minimal inflammation, 2 represented moderate inflammation and 3 represented extensive presence of hemosiderin and inflammation or both.

does not perturb the structural conformation of HFn (Fig. 1(e)), we investigated the binding characteristics using FITC-conjugated HFn nanocages. As shown in Fig. 5(a), immunofluorescent staining of human carotid plaques demonstrated colocalization of FITC-conjugated HFn staining with plaque macrophages (CD 68 staining, Fig. 5(a), upper panels), indicating that HFn specifically binds to macrophages within unstable plaques. We further demonstrated that M-HFn nanozymes specifically binds to plaque macrophages via transferrin receptor 1 (TfR1), which is highly expressed in plaque macrophages (Fig. 5(a), below planels) and significantly associated with the increasing risk of plaque rupture [35]. As shown in Figs. 5(b) and 5(c), the characterization of M-HFn binding to macrophages was investigated using THP-1 human macrophages. FITC-conjugated HFn specifically bound to macrophage cells and the binding could be substantially inhibited by adding an excess of anti-TfR1 monoclonal antibody as determined by both confocal (Fig. 5(b)) and flow cytometric studies (Fig. 5(c)), showing that TfR1 mediates the specific binding of HFn to macrophages. Further saturation binding experiments and Scatchard analysis demonstrated that the K_d value for HFn binding to macrophages was 60.1 nM (Fig. 5(d)) and the total binding capacity B_{max} was 38.7×10^{-19} mol/cell, indicating that HFn has a high binding affinity and capacity for plaque macrophages. The binding capacity of HFn with plaque-infiltrated macrophages is higher than with some tumor cells [36], showing the potential of HFn for plaque macrophage identification.

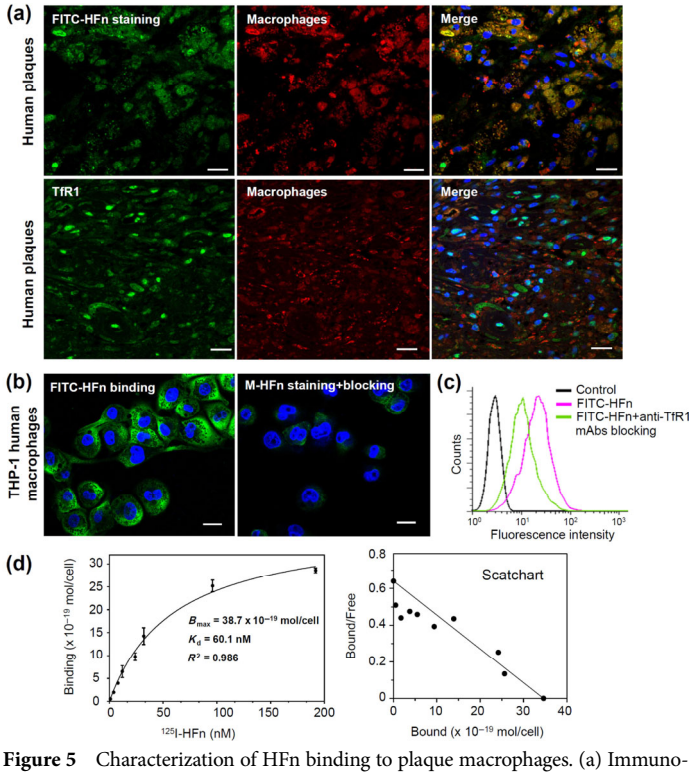

Figure 5 Characterization of HFn binding to plaque macrophages. (a) Immunofluorescent staining of human carotid plaques demonstrated colocalization of FITC-conjugated HFn and anti-TfR1 staining with macrophages (CD68 staining) within plaques (scale bars, 20 μm). (b) Confocal analysis of FITC-conjugated HFn staining of human macrophages in the presence (right) or absence (left) of a 10-fold molar excess of anti-TfR1 mAbs (scale bars, 20 μm). (c) Flow cytometric analysis of the binding of FITC-conjugated HFn to TfR1 in human macrophages with or without a 10-fold molar excess of anti-TfR1 mAbs ($n = 3$, bars represent means ± SD). (d) FITC-conjugated HFn bound to human macrophages with a K_d value of 60.1 nM and a total binding capacity B_{max} of 38.7×10^{-19} mol/cell.

3 Discussion

Inflammation drives the formation, progression, and rupture of atherosclerotic plaques and is typically characterized by the presence of macrophages within plaques [5, 32, 34]. We previously reported that human HFn specifically binds to human cells via TfR1 [27], which is highly expressed in the plaque-infiltrated macrophages and significantly associated with the instability and rupture of human atherosclerotic plaques [35]. The findings in this study show that the bioengineered HFn can specifically recognize high-risk and ruptured human atherosclerotic plaques via specific binding to macrophage-expressed TfR1 within atherosclerotic plaques (Figs. 5(a)–5(c)). We further identified that the radiolabeled HFn bound to human macrophages with high specific binding affinity ($K_d = 60.1$ nM) and capacity ($B_{max} = 38.7 \times 10^{-19}$ mol/cell) (Fig. 5(d)).

After loading iron nanocores within HFn nanocages, the bioengineered M-HFn NPs functionally mimiced peroxidase enzymes and achieved one-step pathological staining of high-risk and ruptured plaques from patients with symptomatic carotid disease (Fig. 3). Even more importantly, it was found that M-HFn staining displayed a significant correlation with plaque vulnerability ($r = 0.89$, $P < 0.0001$) (Fig. 4). Our results thus support that M-HFn staining can be used as a clinical index for human unstable and ruptured plaque identification.

In comparison with the conventional immunohistochemical methods, the M-HFn nanozyme staining method described herein presents two important points of advantages: (1) Low-cost: HFn nanocages are produced from *E. coli* with a high yield (> 100 mg/L from the bacterial lysate) [27], and M-HFn nanozymes can be mass produced by biomining iron within HFn nanocages [28]. (2) Simplicity and speed: Achieving rapid, low-cost and specific pathological identification of high-risk unstable atherosclerotic plaques remains a challenge due to the complexities of this disease. This study shows that one-step pathological staining of high-risk plaques with low-cost and mass-produced M-HFn nanozymes is feasible for convenient monitoring and analysis of high-risk plaques from patients with acute coronary events and symptomatic carotid vascular disease.

4 Conclusions

This study reports the feasibility for pathological identification of high-risk and ruptured plaques with M-HFn nanozymes, and demonstrates that M-HFn staining displayed a significant correlation with plaque vulnerability. The cell studies in human macrophages indicated that HFn specifically binds to plaque macrophages via TfR1, which is highly expressed in plaque macrophages and significantly associated with the increasing risk of plaque rupture. With the obvious advantages of simplicity and speed of M-HFn staining for identification of plaque vulnerability, we believe clinical employment of M-HFn nanozymes would demonstrate superior pathological staining characteristics.

5 Materials and methods

5.1 Preparation and characterization of M-HFn nanozymes

Recombinant human heavy-chain ferritin (HFn) was produced in *E. coli* and purified as previously described [31, 37]. Briefly, *E. coli* lysate expressing HFn was centrifuged at 10,000*g* for 30 min. The supernatant was then heated for 10 min at 70 °C to precipitate unwanted proteins. After centrifugation, the supernatant was precipitated by ammonium sulfate (520 g/L). The precipitates were collected by centrifugation and re-dissolved in PBS. After dialyzing out the remaining ammonium sulfate, HFn nanocages were sequentially purified by Q sepharose Fast Flow ion exchange column (GE Healthcare) followed by the size-exclusion chromatography on a superdexTM 200 10/300 GL column (GE Healthcare). Concentration of HFn was determined by BCA protein assay kit (Pierce). The final yield of HFn was >100 mg/L from the bacterial lysate. Iron oxide nanocore was synthesized within HFn nanocage by the procedures described previously [27].

Iron oxide nanocore was synthesized within HFn nanocage by the following procedures described below. Briefly, a solution of HFn (0.2 mg/mL in 50 mL of 100 mM NaCl) was added to the reaction vessel with the temperature kept at 65 °C and the pH titrated to 8.5. Iron(II) (25 mM $(NH_4)2Fe(SO_4)_2{\cdot}6H_2O$) was added as iron source at a rate of 100 Fe/HFn per minute to attain a theoretical loading factor of 2,300 Fe molecules per protein. Simultaneously, fresh prepared H_2O_2 was added at a stoichiometric equivalent of 1:3 as an oxidant. The synthesized M-HFn was centrifuged to remove aggregation and dialyzed against phosphate-buffered saline overnight.

The prepared M-HFn nanozymes were characterized using cryoelectron transmission microscopy (cryo-EM), dynamic light scattering (DLS), X-ray diffraction (XRD) and circular dichroism (CD) spectroscopy, respectively. For cryo-EM characterization, the purified M-HFn or HFn samples were applied to a holey grid and frozen by FEI Vitrobot. The frozen samples were imaged in a FEI 300 kV with a Gatan Ultrascan 4000, model 895 CCD-camera at the magnification of 96,000 and dose of 20–25 $e^-/Å^2$. CD spectra was acquired on an Applied Photophysics Chirascan Plus spectrometer at 25 °C. The sample concentrations used were 0.25 mg/mL in PBS buffer. The spectra were measured from 280 to 200 nm with 0.1-nm resolution in a quartz cell with a 1 cm path length.

DLS was used to measure the hydrodynamic diameter of HFn nanocages and M-HFn NPs using a DynaPro Titan system DLS instrument (Wyatt Technology). The analysis was performed at 25 °C and the concentration of the samples used was 0.25 mg/mL in PBS buffer. Measurements were collected at 10 s intervals. Each sample was run 10 times.

XRD patterns of the lyophilized M-HFn and HFn samples were obtained on an X-ray diffractometer (computerized Bruker D8 ADVANCE) using Cu Kα radiation source (λ = 0.154 nm). The patterns were taken over the 2θ range from 10° to 90° at a scan speed of 6° per min.

The enzyme-like activity of M-HFn nanozymes was characterized at room temperature. Briefly, M-HFn solution of 0.5 μM was mixed with 500 mM H_2O_2 in 0.2 M sodium acetate buffer (pH 4.5), using 0.2 mg/mL of 3,3′,5,5′-tetramethylbenzidine (TMB, Sigma), 3,3′-diaminobenzidine tetrahydrochloride (DAB, Amresco) or OPD (Sigma) as the substrate. Color reaction was recorded 30 min after addition of the color substrate.

5.2 Labeling of HFn nanocages

HFn was labelled by fluorescein isothiocyanate (FITC, Sigma) using the following procedures. Briefly, FITC was dissolved in dry dimethylformamide (Sigma) and added to 0.1 M $NaHCO_3$ buffered (pH = 8.5) HFn solution. The reaction solution was gently stirred overnight at 4 °C in the dark and then purified on a polyacrylamide column (Thermo Scientific, MWCO 6,000) using 0.1 M PBS, pH = 7.5 to remove free dyes. The concentration of labelled FITC was determined by measuring the absorbance at 492 nm, and the concentration of HFn was measured by BCA reagent kit (Bio-Rad).

Radioiodination of HFn was performed using the lodogen method [38]. Briefly, 0.5 mCi of ^{125}I (Beijing Atom High Tech) was mixed with 100 μg HFn in 100 μL PBS buffer (0.2 M, oH 7.4) and then added into a vial coated with 50 μg Iodogen (Sigma). After incubation for 10 min at room temperature, the mixture was purified with a PD-10 column (Amersham). The final radiochemical yield of ^{125}I-labeled HFn (^{125}I-HFn) was measured by instant thin-layer chromatography (ITLC) using 85% (v/v) methanol as eluant on a radio-thin layer scanner (Bioscan).

5.3 Histological examinations

The human atherosclerotic aorta specimens were obtained from Peking University Third Hospital. Studies were approved by the clinical research ethics committees of Peking University Third Hospital and all patients provided informed consent. Carotid endarterectomy (CEA) was performed using standard surgical techniques with minimal handling of the specimens. The freshly isolated aortas were fixed in 4% Perfluoroalkoxy alkane, dehydrated in 70% ethanol, embedded in paraffin, and sliced in the region that presented obvious plaques. Tissue samples were cut into serial sections 5-μm thick and stained with hematoxylin-eosin for general morphology characterization and Masson for collagen distribution identification. After hematoxylin-eosin and Masson staining, the sections were further assessed by M-HFn staining. Briefly, 1 mg/mL of M-HFn in 5% goat serum was used to incubate the tissue sections overnight. After washing with PBS for 3 times, freshly prepared DAB was added for color development. Digital images of the stained sections were obtained with a scanning light microscope (Leica Microsystems). Two independent pathologists without prior access to the clinical information scored all specimens.

Fluorescence staining of plaque sections was performed to confirm the binding specificity of HFn to macrophages within plaques. Briefly, serial sections were incubated overnight with FITC-conjugated HFn, anti-human TfR1 (Sigma), or a Cy5.5-conjugated anti-human CD68 (abcam). The nuclei were counterstained with 4′,6-diamidino-2-phenylindole. The stained tissues were examined under a confocal laser scanning microscope (Olympus).

5.4 Macrophage culture studies

The human monocytic THP-1 cell line was obtained from the American Type Culture Collection (ATCC) and maintained in RPMI 1640 containing 10% fetal calf serum, penicillin (100 U/mL) and streptomycin (100 μg/mL) at 37 °C with 5% CO_2. We differentiated THP-1 monocytes to macrophages by treating the cells with 100 nM of 1-methoxy-2-propyl acetate (PMA) for 24 h, and then the medium was replaced with serum-free medium containing ox-LDL (50 mg/mL) for 48 h to fully differentiate THP-1 to macrophages before their use in experiments.

The macrophage binding study of HFn was determined by saturation binding experiments. Briefly, THP-1 cells induced by PMA seeded in 48-well plates were incubated in triplicate with increasing concentrations of 125I-HFn (from 0 to 200 nM) in PBS containing 1% bovine serum albumin for 2 h at 37 °C. After incubation, the cells were filtered, washed three times with PBS, and collected, and the radioactivity was determined using a gamma counter (CRC-15 R). Nonspecific binding was determined in the presence of an excess of cold HFn (> 100-fold). A saturation binding curve and Scatchard transformation were obtained by nonlinear regression analysis, and the K_d and B_{max} (maximum number of binding

sites) values of ^{125}I-HFn were calculated using GraphPad Prism 6.0 software. Data were expressed as the average of triplicate samples.

The HFn binding characterization to TfR1 on macrophages was determined by antibody blocking study using THP-1 macrophages induced by PMA. Briefly, 0.3 μM of FITC-conjugated HFn was incubated with THP-1 macrophages in the presence or absence of a 10-fold molar excess of anti-TfR1 antibody. After incubation for 1 h on ice, the cells were washed three times in cold PBS and then collected. Cell-bound fluorescence was measured by a FACS Calibur flow cytometer (Becton Dickinson). To further characterize the binding specificity, the incubated cells were further stained with 4',6-diamidino-2-phenylidole (DAPI, 1 μg/mL, Roche Applied Science) and examined with confocal laser scanning microscope (Olympus FluoView FV-1000) after washing three times in PBS.

5.5 Statistical analysis

All statistical analyses were performed with SPSS19.0 (IBM SPSS Statistics) and GraphPad Prism 6.0 (GraphPad Software Inc.) software. Results were expressed as mean ± SD (n = 3 per group). Statistical analysis was carried out using the unpaired Student's t-test. Correlations between M-HFn staining and plaque vulnerability were determined using the Pearson's coefficient (r) and P value.

Acknowledgements

This work was supported by the following grants: the National Key R&D Program of China (No. 2017YFA0205501), the National Natural Science Foundation of China (Nos. 81722024 and 81571728), the Key Research of Frontier Sciences (No. QYZDY-SSW-SMC013), and Youth Innovation Promotion Association of Chinese Academy of Sciences (No. 2014078).

References

[1] Otsuka, F.; Kramer, M. C. A.; Woudstra, P.; Yahagi, K.; Ladich, E.; Finn, A. V.; de Winter, R. J.; Kolodgie, F. D.; Wight, T. N.; Davis, H. R. et al. Natural progression of atherosclerosis from pathologic intimal thickening to late fibroatheroma in human coronary arteries: A pathology study. *Atherosclerosis* **2015**, *241*, 772–782.

[2] Hansson, G. K. Inflammation, atherosclerosis, and coronary artery disease. *New Engl. J. Med.* **2005**, *352*, 1685–1695.

[3] Narula, J.; Nakano, M.; Virmani, R.; Kolodgie, F. D.; Petersen, R.; Newcomb, R.; Malik, S.; Fuster, V.; Finn, A. V. Histopathologic characteristics of atherosclerotic coronary disease and implications of the findings for the invasive and noninvasive detection of vulnerable plaques. *J. Am. Coll. Cardiol.* **2013**, *61*, 1041–1051.

[4] Virmani, R.; Kolodgie, F. D.; Burke, A. P.; Farb, A.; Schwartz, S. M. Lessons from sudden coronary death: A comprehensive morphological classification scheme for atherosclerotic lesions. *Arterioscler. Thromb. Vasc. Biol.* **2000**, *20*, 1262–1275.

[5] Libby, P.; Ridker, P. M.; Maseri, A. Inflammation and atherosclerosis. *Circulation* **2002**, *105*, 1135–1143.

[6] Moore, K. J.; Sheedy, F. J.; Fisher, E. A. Macrophages in atherosclerosis: A dynamic balance. *Nat. Rev. Immunol.* **2013**, *13*, 709–721.

[7] Libby, P. Inflammation in atherosclerosis. *Nature* **2002**, *420*, 868–874.

[8] Moore, K. J.; Tabas, I. Macrophages in the pathogenesis of atherosclerosis. *Cell* **2011**, *145*, 341–355.

[9] Terashima, M.; Uchida, M.; Kosuge, H.; Tsao, P. S.; Young, M. J.; Conolly, S. M.; Douglas, T.; McConnell, M. V. Human ferritin cages for imaging vascular macrophages. *Biomaterials* **2011**, *32*, 1430–1437.

[10] Rogers, I. S.; Tawakol, A. Imaging of coronary inflammation with fdg-pet: Feasibility and clinical hurdles. *Curr. Cardiol. Rep.* **2011**, *13*, 138–144.

[11] Stone, G. W.; Maehara, A.; Lansky, A. J.; de Bruyne, B.; Cristea, E.; Mintz, G. S.; Mehran, R.; McPherson, J.; Farhat, N.; Marso, S. P. et al. A prospective natural-history study of coronary atherosclerosis. *N. Engl. J. Med.* **2011**, *364*, 226–235.

[12] Tahara, N.; Mukherjee, J.; De Haas, H. J.; Petrov, A. D.; Tawakol, A.; Haider, N.; Tahara, A.; Constantinescu, C. C.; Zhou, J.; Boersma, H. H. et al. 2-Deoxy-2-[^{18}F] fluoro-$_D$-mannose positron emission tomography imaging in atherosclerosis. *Nat. Med.* **2014**, *20*, 215–219.

[13] Weissleder, R.; Nahrendorf, M.; Pittet, M. J. Imaging macrophages with nanoparticles. *Nat. Mater.* **2014**, *13*, 125–138.

[14] Lobatto, M. E.; Claudia, C.; Millon, A.; Senders, M. L.; Fay, F.; Robson, P. M.; Ramachandran, S.; Binderup, T.; Paridaans, M. P. M.; Sensarn, S. et al. Atherosclerotic plaque targeting mechanism of long-circulating nanoparticles established by multimodal imaging. *ACS Nano* **2015**, *9*, 1837–1847.

[15] Li, X.; Wang, C.; Tan, H.; Cheng, L. L.; Liu, G. B.; Yang, Y.; Zhao, Y. Z.; Zhang, Y. Q.; Li, Y. L.; Zhang, C. F. et al. Gold nanoparticles-based SPECT/CT imaging probe targeting for vulnerable atherosclerosis plaques. *Biomaterials* **2016**, *108*, 71–80.

[16] Tonga, G. Y.; Jeong, Y.; Duncan, B.; Mizuhara, T.; Mout, R.; Das, R.; Kim, S. T.; Yeh, Y. C.; Yan, B.; Hou, S. et al. Supramolecular regulation of bioorthogonal catalysis in cells using nanoparticle-embedded transition metal catalysts. *Nat. Chem.* **2015**, *7*, 597–603.

[17] Wang, X. Y.; Hu, Y. H.; Wei, H. Nanozymes in bionanotechnology: From sensing to therapeutics and beyond. *Inorg. Chem. Front.* **2016**, *3*, 41–60.

[18] Liu, B. W.; Liu, J. W. Surface modification of nanozymes. *Nano Res.* **2017**, *10*, 1125–1148.

[19] Wei, H.; Wang, E. K. Nanomaterials with enzyme-like characteristics (nanozymes): Next-generation artificial enzymes. *Chem. Soc. Rev.* **2013**, *42*, 6060–6093.

[20] Gao, N.; Dong, K.; Zhao, A. D.; Sun, H. J.; Wang, Y.; Ren, J. S.; Qu, X. G. Polyoxometalate-based nanozyme: Design of a multifunctional enzyme for multi-faceted treatment of Alzheimer's disease. *Nano Res.* **2016**, *9*, 1079–1090.

[21] Wang, Z. Z.; Zhang, Y.; Ju, E. G.; Liu, Z.; Cao, F. F.; Chen, Z. W.; Ren, J. S.; Qu, X. G. Biomimetic nanoflowers by self-assembly of nanozymes to induce intracellular oxidative damage against hypoxic tumors. *Nat. Commun.* **2018**, *9*, 3334.

[22] Wei, H.; Wang, E. K. Fe_3O_4 magnetic nanoparticles as peroxidase mimetics and their applications in H_2O_2 and glucose detection. *Anal. Chem.* **2008**, *80*, 2250–2254.

[23] Feng, L. Z.; Dong, Z. L.; Liang, C.; Chen, M. C.; Tao, D. L.; Cheng, L.; Yang, K.; Liu, Z. Iridium nanocrystals encapsulated liposomes as near-infrared light controllable nanozymes for enhanced cancer radiotherapy. *Biomaterials* **2018**, *181*, 81–91.

[24] Gao, L. Z.; Zhuang, J.; Nie, L.; Zhang, J. B.; Zhang, Y.; Gu, N.; Wang, T. H.; Feng, J.; Yang, D. L.; Perrett, S. et al. Intrinsic peroxidase-like activity of ferromagnetic nanoparticles. *Nat. Nanotechnol.* **2007**, *2*, 577–583.

[25] Liang, M. M.; Fan, K. L.; Pan, Y.; Jiang, H.; Wang, F.; Yang, D. L.; Lu, D.; Feng, J.; Zhao, J. J.; Yang, L. et al. Fe_3O_4 magnetic nanoparticle peroxidase mimetic-based colorimetric assay for the rapid detection of organophosphorus pesticide and nerve agent. *Anal. Chem.* **2012**, *85*, 308–312.

[26] Zhuang, J.; Fan, K. L.; Gao, L. Z.; Lu, D.; Feng, J.; Yang, D. L.; Gu, N.; Zhang, Y.; Liang, M. M.; Yan, X. Y. *Ex vivo* detection of iron oxide magnetic nanoparticles in mice using their intrinsic peroxidase-mimicking activity. *Mol. Pharm.* **2012**, *9*, 1983–1989.

[27] Fan, K. L.; Cao, C. Q.; Pan, Y. X.; Lu, D.; Yang, D. L.; Feng, J.; Song, L. N.; Liang, M. M.; Yan, X. Y. Magnetoferritin nanoparticles for targeting and visualizing tumour tissues. *Nat. Nanotechnol.* **2012**, *7*, 459–464.

[28] Zhao, Y. Z.; Liang, M. M.; Li, X.; Fan, K. L.; Xiao, J.; Li, Y. L.; Shi, H. C.; Wang, F.; Choi, H. S.; Cheng, D. F. et al. Bioengineered magnetoferritin nanoprobes for single-dose nuclear-magnetic resonance tumor imaging. *ACS Nano* **2016**, *10*, 4184–4191.

[29] Fan, K. L.; Xi, J. Q.; Fan, L.; Wang, P. X.; Zhu, C. H.; Tang, Y.; Xu, X. D.; Liang, M. M.; Jiang, B.; Yan, X. Y. et al. *In vivo* guiding nitrogen-doped carbon nanozyme for tumor catalytic therapy. *Nat. Commun.* **2018**, *9*, 1440.

[30] Xu, Z. B.; Qiu, Z. Y.; Liu, Q.; Huang, Y. X.; Li, D. D.; Shen, X. G.; Fan, K. L.; Xi, J. Q.; Gu, Y. H.; Tang, Y. et al. Converting organosulfur compounds to inorganic polysulfides against resistant bacterial infections. *Nat. Commun.* **2018**, *9*, 3713.

[31] Liang, M. M.; Fan, K. L.; Zhou, M.; Duan, D. M.; Zheng, J. Y.; Yang, D. L.; Feng, J.; Yan, X. Y. H-ferritin–nanocaged doxorubicin nanoparticles specifically target and kill tumors with a single-dose injection. *Proc. Natl. Acad. Sci. USA* **2014**, *111*, 14900–14905.

[32] Ross, R. Atherosclerosis—An inflammatory disease. *N. Engl. J. Med.* **1999**, *340*, 115–126.
[33] Ding, J. L.; Wang, Y. H.; Ma, M.; Zhang, Y.; Lu, S. S.; Jiang, Y. N.; Qi, C. M.; Luo, S. H.; Dong, G.; Wen, S. et al. CT/fluorescence dual-modal nanoemulsion platform for investigating atherosclerotic plaques. *Biomaterials* **2013**, *34*, 209–216.
[34] Chinetti-Gbaguidi, G.; Colin, S.; Staels, B. Macrophage subsets in atherosclerosis. *Nat. Rev. Cardiol.* **2015**, *12*, 10–17.
[35] Li, W.; Xu, L. H.; Forssell, C.; Sullivan, J. L.; Yuan, X. M. Overexpression of transferrin receptor and ferritin related to clinical symptoms and destabilization of human carotid plaques. *Exp. Biol. Med.* **2008**, *233*, 818–826.
[36] Fargion, S.; Arosio, P.; Fracanzani, A. L.; Cislaghi, V.; Levi, S.; Cozzi, A.; Piperno, A.; Fiorelli, G. Characteristics and expression of binding sites specific for ferritin h-chain on human cell lines. *Blood* **1988**, *71*, 753–757.
[37] Liang, M. M.; Tan, H.; Zhou, J.; Wang, T.; Duan, D. M.; Fan, K. L.; He, J. Y.; Cheng, D. F.; Shi, H. C.; Choi, H. S. et al. Bioengineered H-ferritin nanocages for quantitative imaging of vulnerable plaques in atherosclerosis. *ACS Nano* **2018**, *12*, 9300–9308.
[38] Salacinski, P. R. P.; McLean, C.; Sykes, J. E. C.; Clement-Jones, V. V.; Lowry, P. J. Iodination of proteins, glycoproteins, and peptides using a solid-phase oxidizing agent, 1,3,4,6-tetrachloro-3α,6α-diphenyl glycoluril (iodogen). *Anal. Biochem.* **1981**, *117*, 136–146.